Transport and Communications Science Journal, Vol. 75, Issue 07 (09/2024), 2058-2069

Transport and Communications Science Journal

AERODYNAMIC CHARACTERISTICS OF AXISYMMETRIC BOATTAIL MODELS WITH DIFFERENT NUMBER OF LONGITUDINAL GROOVE CAVITIES

Tran The Hung[1*], Nguyen Dinh Quang[1], Le Dinh Anh[2]

[1]Le Quy Don Technical University, No 236 Hoang Quoc Viet Street, Bac Tu Liem, Hanoi, Vietnam
[2]VNU-University of Engineering and Technology, Vietnam National University (Hanoi) 144 Xuanthuy, Caugiay, Hanoi, Vietnam

ARTICLE INFO

TYPE: Research Article
Received: 31/05/2024
Revised: 04/09/2024
Accepted: 10/09/2024
Published online: 15/09/2024
https://doi.org/10.47869/tcsj.75.7.4

[*] *Corresponding author*
Email: tranthehung_k24@lqdtu.edu.vn; Tel: 0355544745

Abstract. Reducing aerodynamic drag and increasing flying object performance is an important task in aerospace engineering. The high drag occurs for blunt base models, which are not only for missiles, and projectiles but also for building, bridges. This study presents numerical results regarding subsonic flow characteristics over axisymmetric boattail models equipped with longitudinal grooves, with the number of grooves ranging from 2 to 12. The standard model has a fixed boattail length of 0.7*D* and an angle 22°. The investigation employs numerical simulation methods utilizing the Reynolds-averaged Navier-Stokes (RANS) equations with the *k-ω* SST turbulent model. The boundary layer was captured well by the current simulation. The numerical results are initially validated against both simulated and experimental data from previous studies, ensuring accuracy and reliability. The findings indicate that an increase in the number of grooves from 0 to 4 results in a slight increment in drag. However, as the number of grooves is further increased from 6 to 12, a significant reduction in the model's drag is observed. Additionally, the flow patterns around the boattail model are visually depicted and analyzed to explain the drag trend of the model with different groove configurations.

Keywords: Boattail, grooves, axisymmetric boattail model, numerical simulation.

1. INTRODUCTION

In the aerospace industry, various flying devices with a boattail shape can be encountered, such as missiles, aircraft, UAVs, smart bombs, or artillery shells. The purpose of this tail shape is to accommodate equipment on aircraft, missiles, or UAVs, or to increase the efficiency of propellants in artillery shells when fired. However, the flow around the boattail is very complex, often is characterized by a region of negative pressure gradient, significantly large flow separation, and high turbulence. This leads to the generation of a large component of afterbody pressure drag as well as the total drag of the model.

According to Krieger and Vukelich [1], the drag on the tail can account for up to 50% of the total drag of a missile without a jet stream. Similarly, for artillery shells, the drag from the separated flow at the blunt tail can contribute up to 60% of the total drag [2]. Flow separation, along with high turbulence, not only generates significant drag but also increases fuel consumption and causes noise, vibration, instability, and even structural damage to the devices. Therefore, reducing drag for boattail bodies becomes extremely critical.

Numerous studies have explored strategies to diminish base drag, with tail shape enhancement emerging as a cost-effective and straightforward method for boattail bodies. Creating grooves on the boattail surface is seen as a method to significantly reduce drag. These grooves strategically alter the boundary layer's flow dynamics, trapping air and fostering small vortices around the body [3]. These vortices, characterized by significant kinetic energy, extend the airflow rearward along the boattail surface, thereby mitigating flow separation – a phenomenon reminiscent of the drag reduction mechanism observed in shark skin [4], [5]. This technique, akin to nature's optimization, effectively modifies surface flow patterns, resulting in reduced drag and increased velocity. Notably, this method has found application beyond aerospace, with its efficacy demonstrated in naval settings for reducing drag between ships and water [5]. Moreover, researchers have explored its potential for flying objects [3], [6], [7]. Howard et al. [3] proposed groove utilization for symmetric bodies, showcasing through smoke visualization experiments that longitudinal grooves mitigate flow separation and reduce drag. More recent work by Mariotti et al. [6], [8] focused on transverse grooves for symmetric bodies, revealing their effectiveness in curbing flow separation on boattail surfaces, consequently reducing pressure drag.

Furthermore, Ibrahim and Filippone [9] conducted experimental and simulated studies on the utilization of evenly distributed longitudinal grooves on symmetric conical tails. Their findings revealed a modest drag reduction effectiveness (~2% at M = 1.36), indicating the potential but limited efficacy of this approach. Through studies on longitudinal and transverse grooves arranged on the tail surface mentioned above, we can see the feasibility of this method in reducing drag on objects. However, research on grooves is still not specific enough, and the principles for selecting groove parameters and recommendations for the number of grooves have not been clearly explained. The influence of grooves on the flow behind the object and aerodynamic characteristics has not been thoroughly addressed.

Recently, the development of computational technology has provided a powerful tool for analyzing fluid dynamics. Many turbulence models have been developed and have shown high potential in flow analysis. While Reynolds-averaged Navier-Stokes (RANS) equations can describe time-averaged flow economically, large eddy simulation (LES) and direct numerical simulation (DNS) schemes can be used to analyze unsteady flow. However, the use of LES and DNS requires a powerful computer system and consumes a lot of time. In this

paper, the influence of grooves and the number of grooves on drag reduction and flow structure around the boattail will be studied using the Reynolds-averaged Navier-Stokes (RANS) method. The turbulence model (k-ω SST) is used to obtain highly accurate results at the boundary layer while minimizing computational time. Simulation results will be compared with some experimental and simulated results presented in previous publications.

2. NUMERICAL METHOD

2.1. Research model

Figure 1 illustrates the axisymmetric boattail model utilized in this study, along with the computational domain model employed for simulation. The model has a diameter (D) of 30 mm and a total length (L) of 251 mm. Notably, the nose of the model features an elliptical shape, strategically designed to mitigate flow separation on the surface. The boattail has a conical shape with an angle β = 22°, while the boattail length (L_b) remains fixed at 0.7D. The angle is selected because the flow phenomenon on the boattail surface with large separation is generated. The parameters of longitudinal grooves on the boattail include groove diameter (d), groove-peak distance (A), and the grooves cross the tangent line of the boattail surface and the base surface of the tail. The model was made of aluminum. The groove diameter was 9 mm and the groove-peak A is also fixed at 6 mm for all test cases.

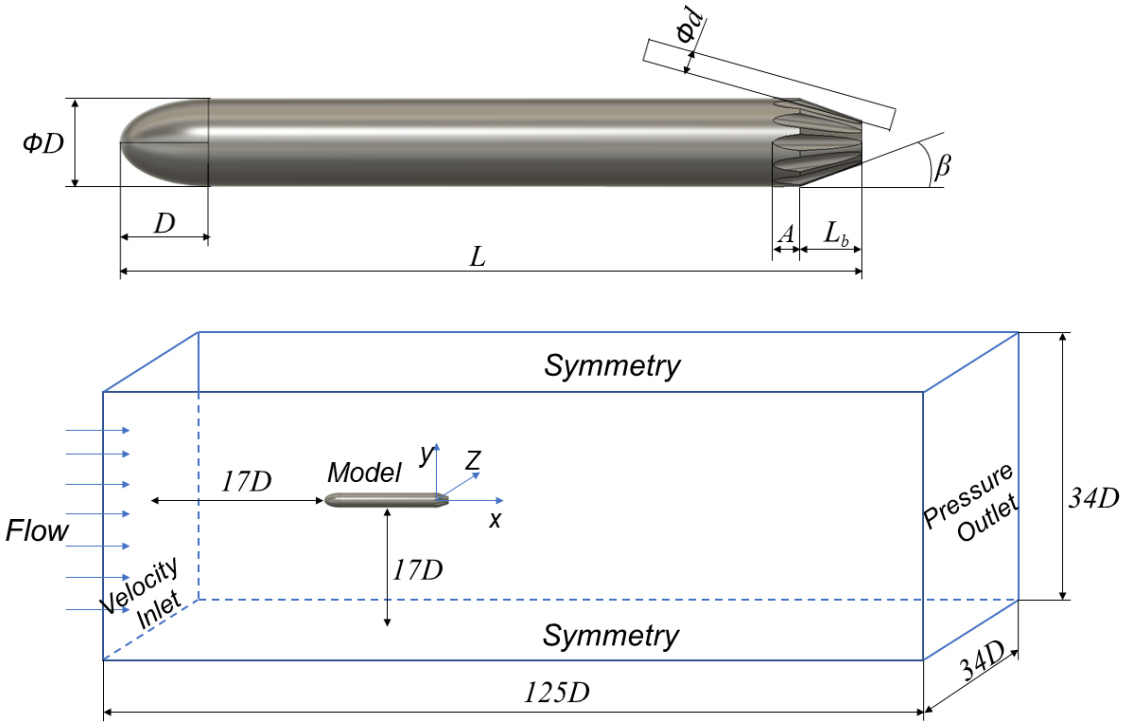

Figure 1. Research model and computational domain.

The computational domain has dimensions of 125D × 34D × 34D corresponding to length, width, and height. An inlet velocity of U_∞ = 22 m/s is applied to the incoming flow plane, at a distance of 17D upstream of the model nose. This velocity choice aligns with previous experimental studies [10], [11], ensuring consistency and facilitating result comparison. Slight variations in velocity have little impact on the flow pattern and external drag of the model except at extreme angles where the flow transitions to a fully separated

state. The Reynolds number based on the model diameter is $Re = 4.34\times10^4$. The boundaries of the computational domain are treated with Symmetry conditions.

2.2. Numerical scheme

In this study, the Reynolds-averaged Navier-Stokes (RANS) equations with the *k-ω* SST turbulence model are applied for numerical simulations. This model combines the *k-ω* model for near-wall flow and the k-ε model for far-wall flow. The *k-ω* SST turbulence model incorporates two additional turbulence equations, *k-ε*, and *k-ω*, to simulate turbulence characteristics [12], allowing for highly accurate results near the surface of the object and reducing computational time in numerical simulations. To derive the RANS equations, the averaging process is applied to the Navier-Stokes equations, including the continuity equation, the three momentum equations, and the energy equation. Specifically, the RANS model can be represented as follows:

$$\frac{\partial \rho}{\partial t} + \frac{\partial}{\partial x_i}\left(\rho u_i\right) = 0 \tag{1}$$

$$\frac{\partial}{\partial t}\left(\rho u_i\right) + \frac{\partial}{\partial x_j}\left(\rho u_i u_j\right) = -\frac{\partial p}{\partial x_i} + \mu \frac{\partial}{\partial x_j}\left(\frac{\partial u_i}{\partial x_j} + \frac{\partial u_j}{\partial x_i}\right) + \frac{\partial}{\partial x_j}\left(-\rho \overline{u_i' u_j'}\right) \tag{2}$$

Where: $i, j = 1, 2, 3$; u_i is the average velocity component in each direction, p is pressure, ρ is air density; $-\rho \overline{u_i' u_j'}$ is Reynolds Shear Stress.

Equations for k and ω are:

$$\frac{\partial\left(\rho k\right)}{\partial t} + \frac{\partial\left(\rho u_j k\right)}{\partial x_j} = P + \beta^* \rho \omega k + \frac{\partial}{\partial x_j}\left[\left(\mu + \sigma_k \mu_t\right)\frac{\partial k}{\partial x_j}\right] \tag{3}$$

$$\frac{\partial\left(\rho \omega\right)}{\partial t} + \frac{\partial\left(\rho u_j \omega\right)}{\partial x_j} = \frac{\gamma}{\nu_t} P - \beta \rho \omega^2 + \frac{\partial}{\partial x_j}\left[\left(\mu + \sigma_k \mu_t\right)\frac{\partial \omega}{\partial x_j}\right] + 2\left(1 - F_1\right)\frac{\rho \sigma_{\omega 2}}{\omega}\frac{\partial k}{\partial x_j}\frac{\partial \omega}{\partial x_j} \tag{4}$$

Here, ν_t is the turbulent viscosity due to eddy viscosity, represented as follows:

$$\nu_t = \frac{a_1 k}{\max(a_1 \omega; \Omega F_2)} \tag{5}$$

In the above equations, P is the production of turbulence kinetic energy, $\sigma_k, \sigma_{\omega 2}, \beta, \beta^*, k, \gamma$ are constants, chosen differently for near-wall and far-from-wall flows.

In this study, we utilized the licensed commercial software ANSYS Fluent for simulation. A non-slip boundary condition on the model is applied to the model surface. The Coupled algorithm was selected with a convergence criterion set at a residual tolerance of 10^{-6}.

2.3. Mesh structure around the model

The computational domain was discretized using an unstructured mesh. The mesh structure on the surfaces of the research model is illustrated in Figure 2 (a, b, c). To conform to the *k-ω* SST turbulence model, the first cell height from the model surface was set at

8.5×10^{-5} m with a growth ratio of 1.18 for subsequent layers. This yielded the y^+ values on the object surface as shown in Figure 2d, with the maximum value approximately close to 6.

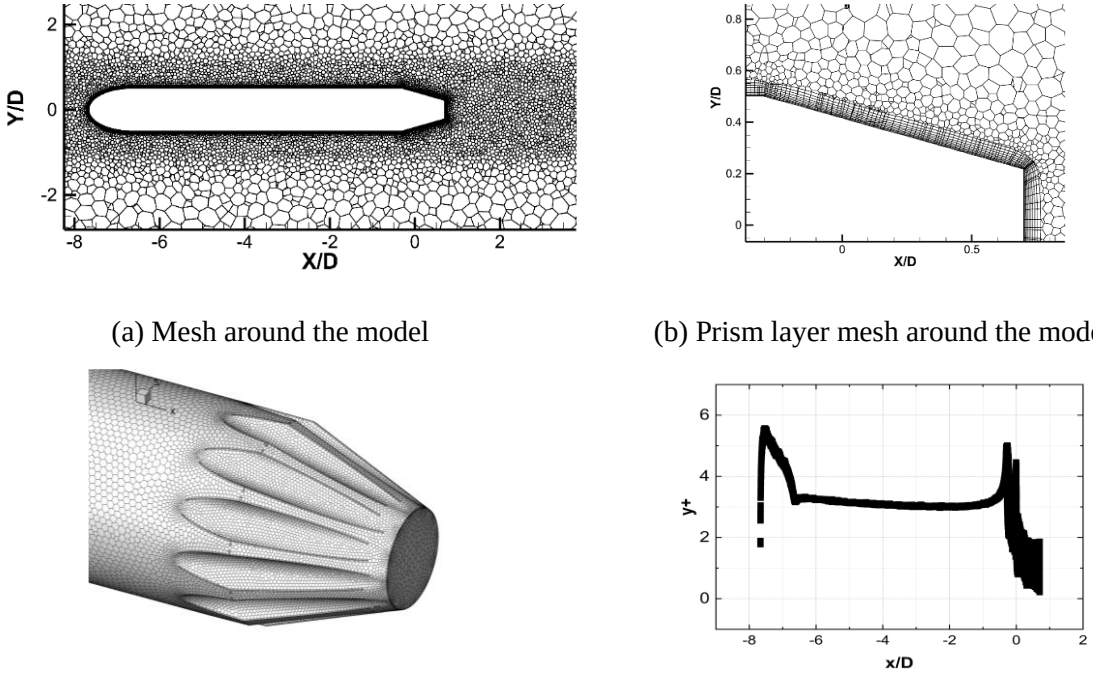

(a) Mesh around the model

(b) Prism layer mesh around the model

(c) Surface mesh of the model

(d) y+ value distribution

Figure 2. Mesh structure and y^+ values.

The convergence of the mesh was checked by incrementally increasing the number of mesh cells from 0.64 million to 4.95 million. The results showed that the values remained almost unchanged when the number of mesh cells reached 3.70 million (Figure 3). Therefore, the 3.70 million cell mesh was selected to ensure good computational results and save computational time.

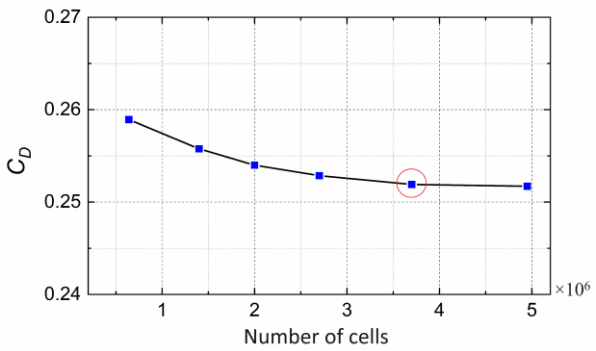

Figure 3. The influence of mesh cells on drag force.

The numerical simulation results were validated by comparing them with the computational results from Tran et al. [13], showing good agreement with an error of ≤ 5.5%, as illustrated in Figure 4. Here, the C_D is the drag coefficient, which can be calculated as $C_D = F_x/(1/2\rho V^2 S)$, with F_x being a total force in the x direction, V is freestream velocity and S is cross-sectional area. These results demonstrate the high accuracy of the computational model, ensuring reliable calculations for other boattail angle models.

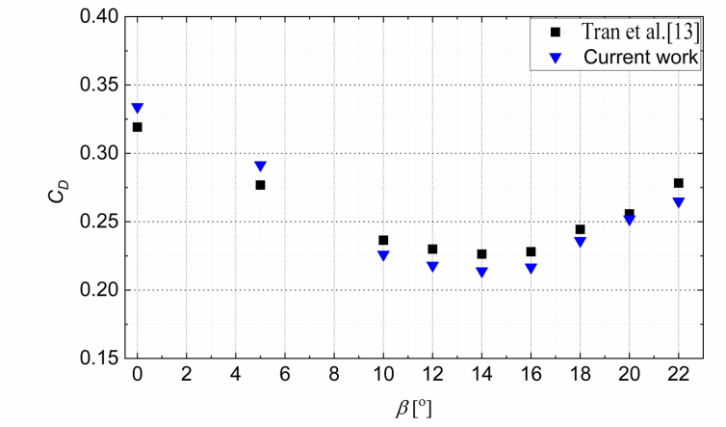

Figure 4. Comparison of drag coefficient results between current work and Tran's results [13].

3. RESULTS AND DISCUSSION

3.1. Influence of number of grooves on drag coefficient

Figure 5 illustrates the drag coefficient values for the axisymmetric model with a 22° boattail angle across varying numbers of grooves. Here, C_{Df} is friction drag coefficient and C_{Dp} is pressure drag coefficient acting on the rear part. These components are integrated from skin friction and pressure acting on the surface in x direction. Notably, the drag coefficient demonstrates a slight increase with a small number of grooves (from 2 to 4 grooves); however, this trend shifts rapidly towards a decrease when the number of grooves exceeds 4. The initial rise in drag with a limited number of grooves presents an intriguing phenomenon, consistent with findings from prior research by Howard et al. [3]. Their investigation highlighted that the drag coefficient of an axisymmetric model with 4 longitudinal grooves would increase within the low Reynolds number region ($Re < 0.08\times10^6$).

Furthermore, the friction drag component remains almost unchanged, while the pressure drag component varies significantly with an increasing number of grooves. The total drag coefficient decreases and reaches its minimum value of C_D = 0.2113 when the number of grooves is 12, equivalent to a reduction of 20.23% compared to the case without grooves.

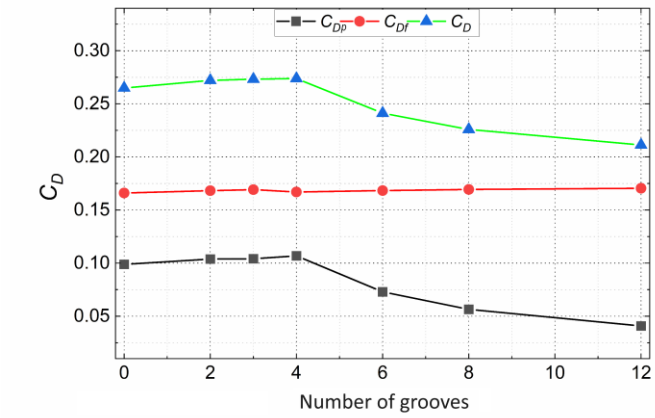

Figure 5. Influence of the number of grooves (n) on the drag coefficient.

3.2. Skin-friction coefficient distribution on boattail surface

The phenomenon of boundary layer separation on the tail surface and on the groove surface can be determined through the analysis of the distribution of the skin-friction coefficient. Specifically, the separation point is identified where the friction coefficient changes from positive to negative, while the reattachment point is where this coefficient changes from negative to positive. This method has been presented in a previous study by Lee et al. [14] for flow around an airfoil using numerical methods. In this study, the skin-friction coefficient is determined by the following equation:

$$C_{fx} = \frac{\mu}{q}\left(\frac{du}{dz}\right)_{z=0} \tag{6}$$

Where, C_{fx} is the skin-friction coefficient in the x direction, μ is viscosity and q is dynamic pressure.

Figure 6 illustrates the skin-friction coefficient of the 22-degree-boattail-angle model with varying numbers of grooves, considering the region with grooves (a) and without grooves (b). It is observed that, in the grooved region, the majority of cases exhibit the coefficient with positive values that indicate no boundary layer separation occurring here. Conversely, in the region without grooves, the opposite trend is observed, with most cases showing negative values of skin-friction coefficient, indicating complete boundary layer separation. However, in cases with a small number of grooves such as 2 or 4 grooves, a reattachment region occurs at the rear of the boattail surface. This could potentially be the cause of increased drag as previously discussed.

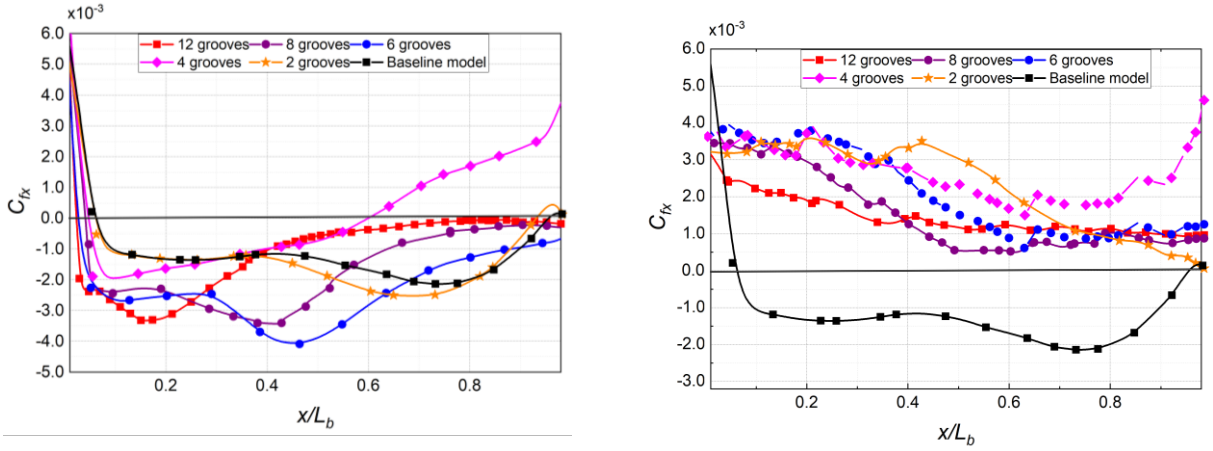

(a) in ungrooved region (b) in grooved region

Figure 6. Skin-friction coefficient of 22-degree-boattail-angle model with varying numbers of grooves.

3.3. Flow structure around boattail

The flow around the boattail for the case of a 22° boattail angle with varying numbers of grooves from 6 to 12 is presented in Figure 7. Notably, in the region with grooves, the flow remains entirely attached across all cases. This phenomenon can be attributed to the reduction in the tapered angle of the model at the groove positions, facilitating smoother flow in these areas. Concurrently, in the ungrooved region, a noticeable decrease in wake flow on the boattail surface is observed with an increasing number of grooves. This reduction in

turbulence may be attributed to the overflow flow from the ungrooved region into the grooved region, thereby reducing the energy of the flow and mitigating turbulent effects. As the number of grooves increases, the prevalence of the overflow phenomenon becomes more pronounced, resulting in minimal turbulent flow occurring on the tail surface in the case of 12 grooves. These observations align closely with the findings reported by Howard et al. [3].

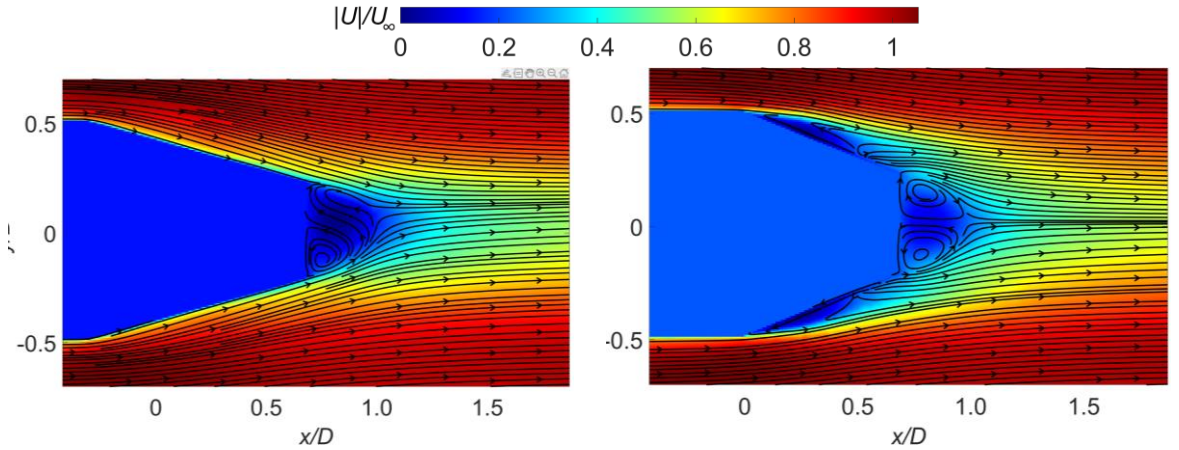

(a) 6 grooves

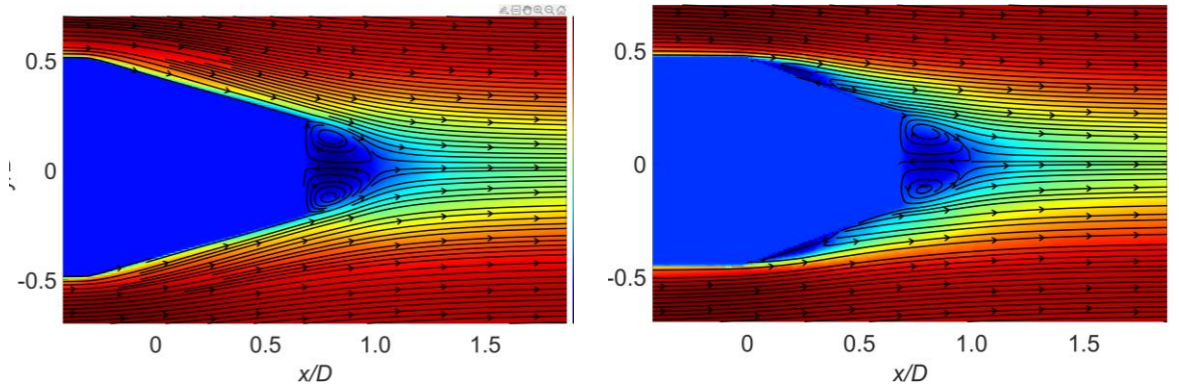

(b) 8 grooves

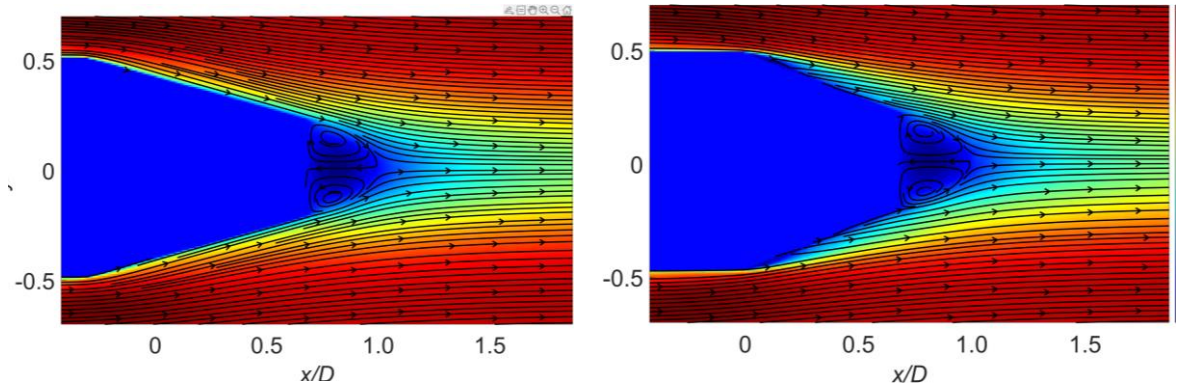

(c) 12 grooves

Figure 7. Flow structure around boattail surface in grooved region (left) and in ungrooved region (right).

3.4. Flow velocity at centerline and recirculation lengths

The flow velocity at the centerline of the near-wake flow is illustrated in Figure 8 for varying numbers of grooves. It is noteworthy that the introduction of grooves on the boattail

surface results in a rapid decrease in the maximum velocity magnitude within the near-wake region. Without grooves, this value reaches approximately 0.4 times the free-stream velocity, consistent with findings by Tran et al. [13] for a 22° angle case. With additional grooves, this value diminishes to approximately 0.15 times the velocity U_∞ for groove numbers ranging from 6 to 12, and even lower for 2 or 4 grooves. This reduction in velocity magnitude corresponds to a decrease in the aerodynamic drag of the model. However, an intriguing observation emerges as the drag force tends to slightly increase in the cases of 2 or 4 grooves.

Similarly, Figure 9 illustrates the values of the length of the recirculation region. Without grooves, the length of the recirculation region reaches approximately 1.1*D*. With the presence of grooves, this length decreases to around 0.2*D* to 0.4*D*. Interestingly, although the recirculation length is smaller in cases with 2 or 4 grooves, the drag coefficient of the model in these scenarios is higher compared to cases with 6 or more grooves, as highlighted in Section 3.1.

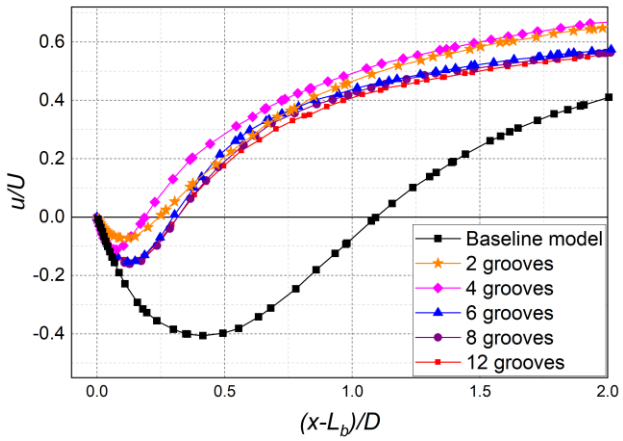

Figure 8. Velocity at centerline for different numbers of grooves.

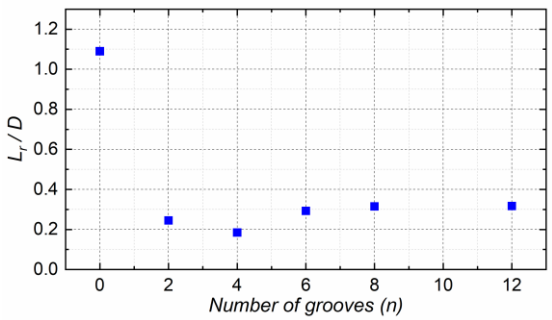

Figure 9. Length of recirculation for different numbers of grooves.

3.5. Pressure distribution along boattail surface

Figure 10 depicts the pressure coefficient (C_p) distribution on the axisymmetric boattail model with a 22° tapered tail, showcasing regions with and without grooves, with varying groove numbers from 2 to 12. We observe that the minimum value of C_p for the baseline case is approximately -0.26. This value is slightly higher in cases with grooves in ungrooved region. However, with the introduction of grooves, there is a notable reduction in C_p values within grooved regions. This is an intriguing phenomenon because with grooves, the taper

angle at the groove position is smaller than the taper angle of the tail without grooves. Specifically, in this case, the taper angle at the groove position is 14.3°.

Nevertheless, this is still consistent with previous research by Tran et al. [13] with $C_p = -0.34$ at a boattail angle of 14°. This phenomenon occurs similarly in cases with different numbers of grooves. Specifically, with 12 grooves, the pressure on the tail surface is highest, followed by cases with 8 and 6 grooves, respectively. In cases with 4 and 2 grooves, the pressure coefficient is essentially lower than the baseline case. This explains why the drag coefficient increases slightly when there are 2 and 4 grooves, as mentioned above.

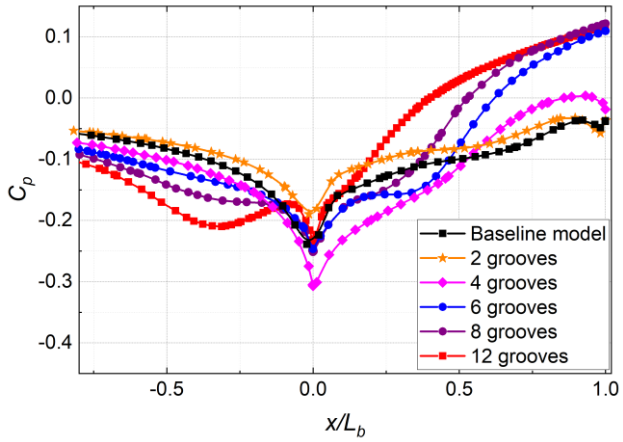

(a) in ungrooved region

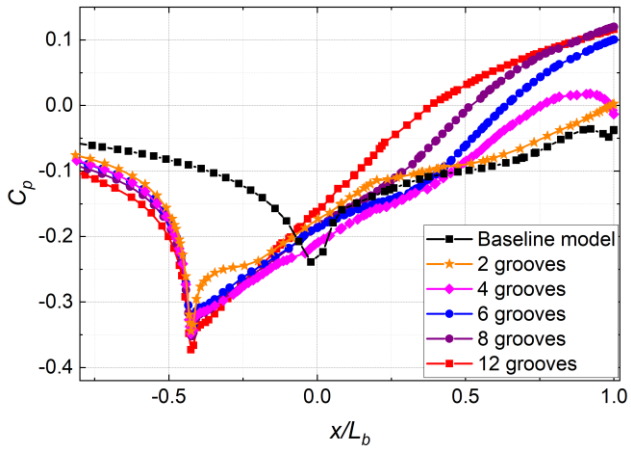

(b) in grooved region

Figure 10. Pressure coefficient of 22° boattail angle model with varying numbers of grooves.

Although this study was conducted only for the 22° boattail model, it is suggested that the groove cavities are also effective for other configurations, where a large separation flow occurs. The results of the current study are, therefore, can be applied practically to other configurations. The reason is from the mechanism of the model in changing the effective angle and thereby the flow behavior on the surface. Additionally, the pressure recovery increase and the drag should be decreased. However, when the separation flow do not occur

on the surface, the use of cavities may have no effect in changing the flow behavior and pressure distribution.

4. CONCLUSION

The influence of longitudinal grooves on the flow structure and the drag of an axisymmetric body with a 22° boattail angle has been specifically investigated in this paper. Using numerical simulation with the *k-ω* SST turbulence model, the study analyzed flow characteristics such as pressure distribution, velocity, and skin-friction of the axisymmetric boattail body with different numbers of grooves (from 2 to 12 grooves) were symmetrically arranged along the tail surface. Consequently, the reasons for the drag reduction compared to the baseline case (the case without grooves) were understood. Through this, the study can draw the following conclusions:

The use of longitudinal grooves on the boattail surface can reduce the drag on the axisymmetric body by up to 20.23% compared to the baseline case. However, the change in drag depends on the number of grooves used; if the number of grooves is less than 4, it may slightly increase the drag. When increasing the number of grooves from 6 grooves, the reduction in the drag coefficient will correspondingly increase.

It is observed that in the grooved region, there is no longer a separation. In the ungrooved areas, the separation region tends to diminish when the number of grooves increase. The pressure increases significantly and the wake of the model becomes smaller for the model with groove cavities. This explains for the reduction of the drag coefficient.

The use of longitudinal grooves is an effective method to reduce drag for axisymmetric boattail bodies without significantly altering their shape. However, other parameters of the grooves such as groove diameter (*d*) and distance from the leading edge (*A*) also need further investigation to select the optimal structure for the grooves.

ACKNOWLEDGMENT

This research is funded by Vietnam National Foundation for Science and Technology Development (NAFOSTED) under grant number 107.03-2021.52.

REFERENCES

[1]. R.J. Krieger, S.R. Vukelich, Tactical missile drag, tactical missile aerodynamics, Progress in Astronautical Aeronautic AIAA, 104 (1986) 383–420.
[2]. P. R. Viswanath, Flow management techniques for base and afterbody drag reduction, Progress in Aerospace Science, 32 (1996) 79–129. http://doi.org/10.1016/0376-0421(95)00003-8
[3]. F.G. Howard, W. L. Goodman, Axisymmetric bluff-body drag reduction through geometrical modification, Journal of Aircraft, 22 (1985) 516–522. http://doi.org/10.2514/3.45158
[4]. A.W. Lang, P. Motta, P. Hidalgo, M. Westcott, Bristled shark skin: a microgeometry for boundary layer control, Bioinspiration & Biomimetics, 3 (2008) 046005. http://doi.org/10.1088/1748-3182/3/4/046005
[5]. Y.F. Fu, C.Q. Yuan, X.Q. Bai, Marine drag reduction of shark skin inspired riblet surfaces, Biosurface and Biotribology, 3 (2017) 11–24. https://doi.org/10.1016/j.bsbt.2017.02.001
[6]. A. Mariotti, G. Buresti, G. Gaggini, M.V. Salvetti, Separation control and drag reduction for boat-tailed axisymmetric bodies through contoured transverse grooves, Journal of Fluid Mechanics, 832 (2017) 514–549. http://doi.org/10.1017/jfm.2017.676

[7]. P. Ball, Shark skin and other solutions, Nature, 400 (1999) 6744. http://doi.org/10.1038/22883
[8]. A. Mariotti, G. Buresti, M.V. Salvetti, Separation delay through contoured transverse grooves on a 2D boat-tailed bluff body: Effects on drag reduction and wake flow features, European Journal of Mechanics-B/Fluids, 74 (2019) 351–362. https://doi.org/10.1016/j.euromechflu.2018.09.009
[9]. A. Ibrahim, A. Filippone, Supersonic aerodynamics of a projectile with slot cavities, Aeronautical Journal, 114 (2000) 15–24. https://doi.org/10.1017/S0001924000003493
[10].T.H. Tran, T. Ambo, T. Lee, L. Chen, T. Nonomura, K. Asai, Effect of boattail angles on the flow pattern on an axisymmetric afterbody surface at low speed, Experimental Thermal and Fluid Science, 99 (2018) 324–335. http://doi.org/10.1016/j.expthermflusci.2018.07.034
[11]. T.H. Tran, T. Ambo, T. Lee, T. Ozawa, L. Chen, T. Nonomura, K. Asai, Effect of Reynolds number on flow behavior and pressure drag of axisymmetric conical boattails at low speeds, Expriments in Fluids, 60 (2019) 1–19. http://doi.org/10.1007/s00348-019-2680-y
[12]. F.R. Menter, Two-equation eddy-viscosity turbulence models for engineering applications, AIAA Journal, 32 (1994) 1598–1605. https://doi.org/10.2514/3.12149
[13]. T.H. Tran, H.Q. Dinh, H.Q. Chu, V.Q. Duong, C. Pham, V.M. Do, Effect of boattail angle on near-wake flow and drag of axisymmetric models: a numerical approach, Journal of Mechanical Science and Technology, 35 (2021) 563–573. http://doi.org/10.1007/s12206-021-0115-1
[14]. D. Lee, S. Kawai, T. Nonomura, M. Anyoji, H. Aono, A. Oyama, K. Fujii, Mechanisms of surface pressure distribution within a laminar separation bubble at different Reynolds numbers, Physics of Fluids, 27 (2015). http://doi.org/10.1063/1.4913500